J Mater Sci: Mater Med (2009) 20:1255–1262
DOI 10.1007/s10856-009-3693-5

Finite element predictions compared to experimental results for the effective modulus of bone tissue engineering scaffolds fabricated by selective laser sintering

S. Cahill · S. Lohfeld · P. E. McHugh

Received: 19 October 2007 / Accepted: 8 January 2009 / Published online: 8 February 2009

Abstract A current challenge in bone tissue engineering is to create scaffolds with suitable mechanical properties, high porosity, full interconnectivity and suitable pore size. In this paper, polyamide and polycaprolactone scaffolds were fabricated using a solid free form technique known as selective laser sintering. These scaffolds had fully interconnected pores, minimized strut thickness, and a porosity of approximately 55%. Tensile and compression tests as well as finite element analysis were carried out on these scaffolds. It was found that the values predicted for the effective modulus by the FE model were much higher than the actual values obtained from experimental results. One possible explanation for this discrepancy, viz. the surface roughness of the scaffold and the presence of micropores in the scaffold struts, was investigated with a view to making recommendations on improving FE model configurations for accurate effective property predictions.

1 Introduction

In bone tissue engineering scaffolds, it is important that the scaffold has sufficient mechanical strength and stiffness to provide structural support to the growing tissue, as well as suitable pore size, high surface to volume ratio, sufficient porosity and high pore interconnectivity to allow for the flow of nutrients, removal of waste, cell communication and cell proliferation [1–4]. The scaffold's mechanical properties may be required to be anisotropic and heterogeneous and this requirement will depend on the bone defect it is intended to repair [2]. Also, the external 3D shape of the scaffold will vary according to the external shape of the bone defect.

To satisfy the requirements of high pore interconnectivity and sufficient porosity, the scaffold will require an open cell structure. It is important to have fabricating techniques that allows for a high degree of control over the scaffold's internal architecture as it can influence the scaffold's mechanical properties, porosity, and pore size. Rapid prototyping techniques are potentially useful here, as they can build structures directly from a computer model using a layer by layer additive process. This layer by layer additive process allows for a high degree of control over the structures internal and external architectures. For example, Williams et al. demonstrated how the Selective Laser Sintering (SLS) rapid prototyping technique can be used to developed scaffolds with an external architecture that replicates the anatomy of a pig's condyle [5], while Luxner et al., Chua et al., and Hutmacher et al. have all demonstrated that rapid prototyping techniques could be used to fabricate scaffolds with different and predefined internal architectures [6–8].

Carrying out tests to analyse how a particular scaffold would perform under the complex loading conditions it would experience in vivo is both difficult and time consuming. Therefore, the ability to predict by computational means how a particular scaffold would perform under complex loading would be useful. As the scaffold properties may be required to be both heterogeneous and anisotropic, an idea currently been explored in the literature is to have a library of scaffold structures, with known geometric, mechanical, and fluid flow properties, that can be assembled together according to the needs of the application. Chua et al. have

S. Cahill (✉) · S. Lohfeld · P. E. McHugh
National Centre for Biomedical Engineering Science,
National University of Ireland, Galway, Ireland
e-mail: senancahill@gmail.com

S. Cahill · P. E. McHugh
Department of Mechanical and Biomedical Engineering,
National University of Ireland, Galway, Ireland

demonstrated the feasibility of such a library [7], while Wettergreen et al. have shown the potential use of Finite Element Analysis (FEA) in predicting scaffold properties by using FEA to examine the effective moduli and stress distribution of different scaffolds structures that could be assembled together [9]. However, to the authors knowledge, only Williams et al. [5] and Luxner et al. [6] have reported on comparisons of FE predictions of scaffold performance to actual results obtained from experimental examination and both groups confined their research to FE predictions for the effective modulus. Williams et al. found the experimental moduli of PCL scaffolds fabricated by the SLS to be around twice the FE predictions, while Luxner et al. found FE predictions for the effective moduli to be accurate for some scaffold structures, but to overpredict for other structures. Luxner et al. fabricated their scaffolds using the SLS and Digital Light Processing (DLP) rapid prototyping techniques.

Having a pore size of less than 200 μm has been shown to inhibit bone formation due to cell occlusion and poor vascularisation [10]; conversely having too big a pore size will result in a low surface to volume ratio and poor tissue growth due to insufficient surfaces for cell adhesion. Therefore, it is postulated that the ideal pore diameter is somewhere between 200 and 900 μm [11]. So far, to the author's knowledge, they are no reported comparisons of FE predictions for the effective moduli of bioresorbable scaffolds fabricated using the SLS technique with suitable pore size to actual effective moduli obtained via experimental tests: the scaffolds fabricated by Williams et al. had a pore size greater than 1.5 mm, while Luxner et al. fabricated their scaffolds from polyamide. In order to reduce the pore size and maintain a high porosity in the scaffold, the material feature size of the SLS needs to be minimized. It is possible that with a minimized material feature size, features such as surface roughness and micropores could have a big influence over the scaffolds mechanical properties.

In this paper, we report on scaffolds with suitable pore size that were fabricated using SLS. These scaffolds were analysed using FE and the FE predictions for effective moduli were compared to actual values obtained from compression or tensile tests; the aim was to access FEA as a predictive tool for the mechanical performance of different scaffold structures. Finally, the possibility of improving predictions by taken into account features surface roughness and micropores is explored.

2 Methods

2.1 Materials

In this study, scaffolds are fabricated from polyamide (Duraform, 3D Systems) due to relative ease of processability in the SLS process, and from polycaprolactone (PCL) (Schaetti Fix 352, Schaetti GmbH, Switzerland). PCL is a FDA approved bioresorbable material that may be suited for bone tissue engineering.

2.2 Scaffold fabrication

In the SLS process, parts are fabricated in a build chamber with x, y, and z axes. The xy plane is the horizontal plane, with the x axis parallel to the front wall of the build chamber and the y axis perpendicular to the front wall of the build chamber; the z axis is the vertical direction. During the SLS process, a powder bed is formed in the build chamber and a laser scans across the powder bed in a series of lines parallel to the x-axis, moving slightly in the y direction after each line. As it scans, the laser liquefies and fuses powder material in a selected region of the part chamber determined by to a cross-section in a 3D CAD model of the part being produced. After each cross-section is finished, a layer of powder is spread over the newly sintered layer, and the sintering process begins again. In this way, the part is built up layer by layer.

A major limitation is the minimum feature size achievable with the SLS is the laser spot diameter. In the SLS system used for this study (Sinterstation 2500^{plus}, DTM, USA), the laser spot diameter was 410 μm. However, after optimising the processing parameters using the standard sintering technique in the SLS (the 'fill scan'), it was found that although paths of sintered material, which form the scaffold struts, parallel to the x axis could be achieved with a thickness of around 400 μm, the minimum thickness achievable for struts parallel to the y axis was 1000 μm. This lower resolution was due to more laser energy being applied to the struts sintered parallel to the y axis. This happened as a result of the 'fill scan' method being programmed to sinter in the x direction, meaning that struts sintered parallel to the y axis were not sintered with one continuous application of the laser but a series of bursts of the laser. When the laser sinters along a path, it takes time for the laser to get up to speed; so when it sinters in bursts, it never gets up to speed. Therefore, sintering in bursts means more energy is applied as the laser spends more time sintering a point.

Further examination showed that the so called "outline scan" function in the Sinterstation could be used to make the thickness of struts parallel to the y axis the same as struts for parallel to the x axis [12]. Using this technique, the "WYSIWYG" ("What You See Is What You Get") nature of prototyping machines is no longer applicable. A 3-D model similar to that in Fig. 1a could be entered into the design software of the Sinterstation (Sinter version 3.3) and instead of a 3D replica of the CAD model a structure similar to that in Fig. 1b would be fabricated. This

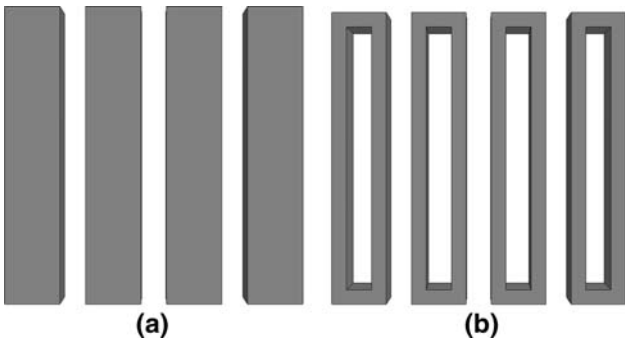

Fig. 1 **a** Designed struts, **b** this is the result of using the "outline scan" function in the sinterstation to fabricate the design in **a**

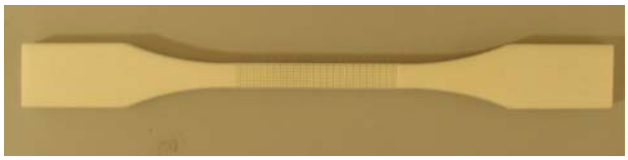

Fig. 2 Specimen used to test the effective modulus of the PA scaffolds in tension

technique, which allows struts in any orientation within the *x*–*y*-plane to be sintered with one continuous application of the laser, was used to fabricate the compressive and tensile PA samples and the compressive PCL samples [12].

For tensile testing of PA samples, scaffold specimen were fabricated similar to the design outline in ASTM standard D638, but due to the used design and manufacturing approach the cross-section had to be changed to 7×7 mm^2 (Fig. 2). To determine the effective moduli of these scaffolds in different directions, tensile specimen were manufactured with their longitudinal axis parallel to the *x*, *y*, and *z* directions. For compression testing, cubic samples of the size $7 \times 7 \times 7$ mm^2 were fabricated (Fig. 3).

For the PCL scaffolds, the design was changed to a cylindrical one. The cylindrical scaffolds were fabricated with five layers having five struts each orientated parallel to the *x* axis and four layers with three struts orientated parallel to the *y* axes. This reduced number of struts resulted from the observation that struts parallel to the *y* axis still had a higher thickness of 600 μm, possibly due to a lower scan speed of the laser bean across the part bed in *y* direction. To keep the pore size consistent in both directions, the number of struts along the *y* axis had to be reduced. The external structures of the PCL samples were cylindrical with a height of 5.5 mm in the *z* direction and a diameter of 5 mm on the *xy* plane (Fig. 4) and were tested in compression. After the scaffolds were fabricated, loose powder was removed from the pores via sandblasting for the PA scaffolds and with compressed air for the PCL scaffolds.

2.3 Mechanical tests

Tensile testing of the cubic PA specimens was carried out on an Instron 8874 Servo-hydraulic Bi-axial Testing System. A 10 kN load cell was used to determine the stress, while a ME46-350 Video Extensometer System (Messphysik, Austria) was used to determine the strain. For the solid samples, strain gauges (Vishay, North Carolina) were used to determine the strain and Poisson's ratio. For all tests, the rate of grip separation was 1 mm/min. Compression tests of both the PA cubic scaffolds and the PCL scaffolds were carried out on a Zwick Z2.5 using a 1 kN load cell and at a compression rate of 1 mm/min. For all scaffold types a minimum of eight samples were tested.

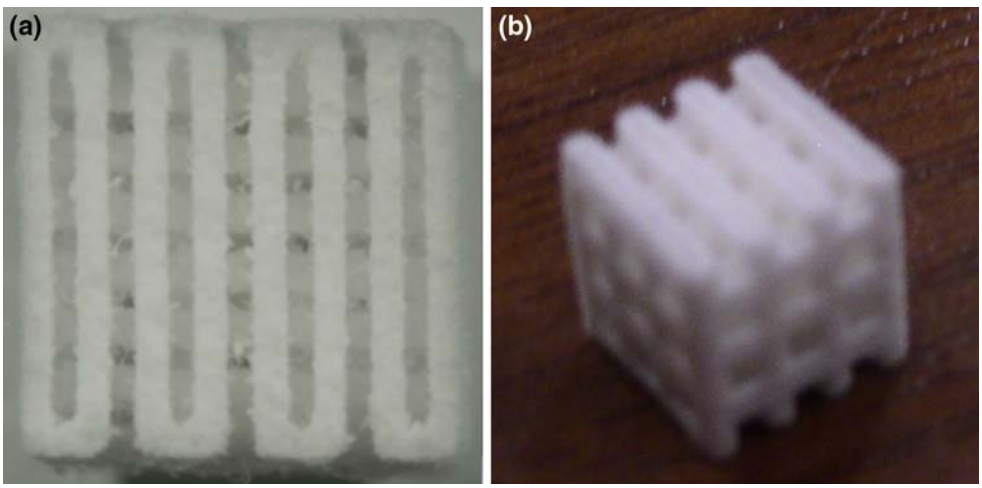

Fig. 3 **a** Top view of PA compressive sample, **b** isometric view of PA compressive sample

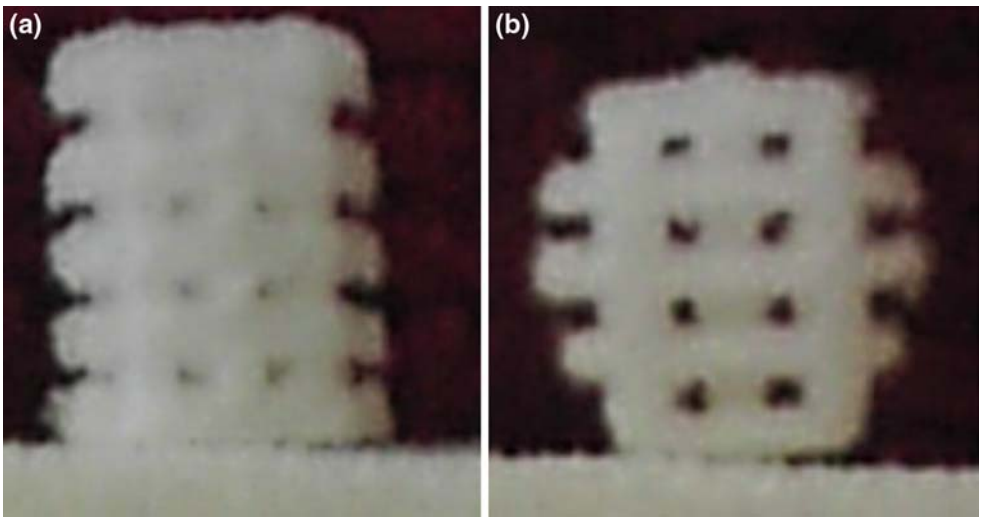

Fig. 4 **a** Side view of PCL compressive sample, **b** top view of PCL compressive sample

2.4 SEM images

To draw up a finite element model which represents the actual prototyped scaffold and not just the intended CAD design, plus to calculate the actual porosity and surface to volume ratio, it was necessary to determine the actual strut thickness. To do this, two PCL and two PA scaffolds were placed in a SEM (S-4700 Hitachi Scientific Instruments, Berkshire, UK) and images were taken of every strut in the surface of each scaffold resulting in eight SEM images been taken of the PA scaffolds and five SEM images been taken of the PCL scaffolds. Then, two parallel lines were drawn which approximated the average strut thickness of the struts in each image and the distance between these two lines was taken to be the average strut thickness of that strut. The distances between the struts were measured using the same technique and taken to be the pore size (Fig. 5).

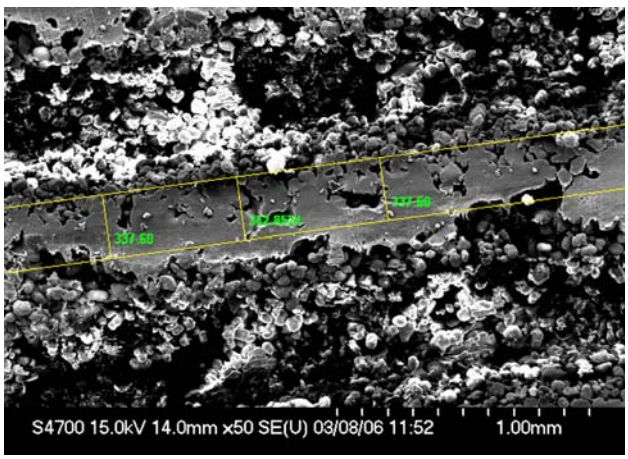

Fig. 5 SEM image of a PA scaffold. The thickness of the strut shown in this image is the distance between the two lines

2.5 The FE model

The scaffolds structures that were modelled are shown in Fig. 6 (PA scaffold) and Fig. 7 (PCL scaffold). In these structures, all struts have equal thickness and are equal distance apart (they have equal pore size), with the values for strut thickness and pore size determined by averaging the measurements taken in the SEM images. These structures were then used to estimate the porosity and the surface to volume ratio of the scaffolds.

The scaffolds were modelled using ABAQUS v6.5. 8-noded linear brick elements were used and each strut had at least four elements across its diameter. To simulate compression tests, all nodes bar one at the bottom end of the

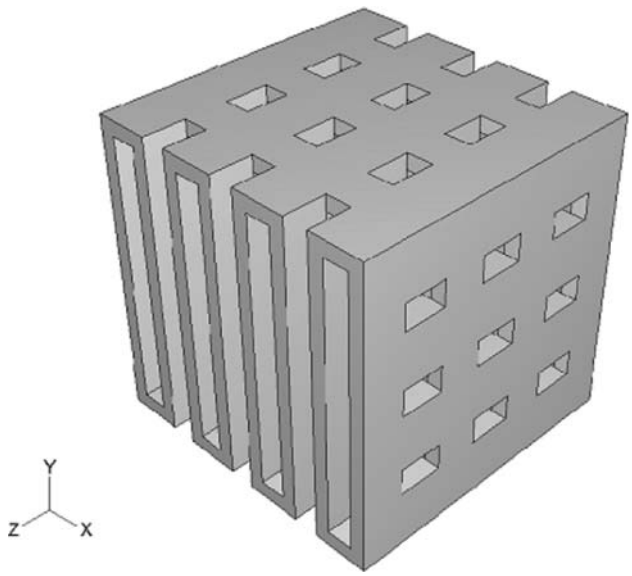

Fig. 6 PA scaffold structure that was modelled

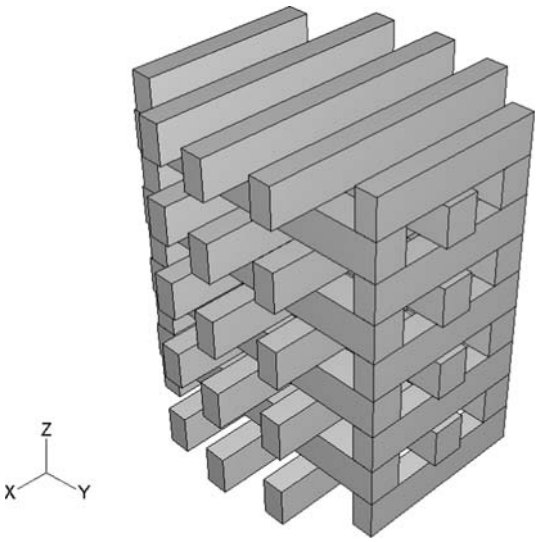

Fig. 7 PCL scaffold structure that was modeled

scaffold were constrained solely in the direction of loading; the remaining node, which was in a corner for the cubic PA scaffolds and close to the centre for the cylindrical PCL scaffolds, was constrained in the x, y, and z directions. At the top end of the scaffold, the nodes were coupled and were given a displacement corresponding to a compressive strain of 1%. The effective modulus of the scaffold was then calculated by inputting the resultant reaction force generated at the top end into Eq. 1

$$\frac{F_{\mathrm{R}}}{A_{\mathrm{CS}}} = E_{\mathrm{effective}} \times \varepsilon_A \tag{1}$$

where F_{R} is the reaction force, A_{cs} is the total cross-sectional area, $E_{\mathrm{effective}}$ is the effective modulus and ε_A is the applied strain.

The FE analysis outlined above was used to predict the effective moduli of the PA scaffolds in the x, y, and z directions and of the cylindrical PCL scaffolds in the direction of their height (z direction).

2.6 Roughness simulation in FE model

To examine if surface roughness influences a scaffold's effective modulus, two scaffolds with the same porosity were modelled as above. These structures had only one difference in their design: one scaffold had struts with a smooth surface (as in the models above) and the other had struts with a rough surface. This rough surface was simulated by randomly varying the width of the scaffold struts in the xy plane, so that their edges were jagged, but the centre of the struts was continuous from end to end. For these models, the materials in both scaffolds were assumed to be isotropic.

2.7 Input data for FE model

Due to the layer-by-layer manufacturing process of SLS, it is possible that the fusion between two successive layers is different from the fusion within one layer [13, 14]. Therefore, it is possible that the elastic modulus in the z direction (direction in which layers are applied) is different from that in the x and y direction (within the layers). In case the mechanical tests reveal that this is true for the present scaffolds, the material properties used in the FE model of the scaffold cannot be assumed to be fully isotropic but only transversely isotropic at best. Assuming transverse isotropy (as is done here) means that five material properties had to be derived from the experiments described above, which are E_x, E_z, G_{xz}, v_{xz}, and v_{zx}, where E_x is the elastic modulus in both the x and y directions, E_z is the elastic modulus in the z direction, G_{xz} is the shear modulus in both the xz and yz planes, v_{xz} is the negative ratio of the strain in the z direction to the x direction for stress applied in the x direction and v_{zx} is the negative ratio of the strain in the x direction to the strain in the z direction for stress applied in the z direction.

E_x, E_z, v_{xz}, and v_{zx} were determined from carrying out tensile tests on solid samples fabricated in x and z direction. Additionally, to verify that the elastic modulus was the same in x and y direction, solid tensile specimens were also fabricated in the y direction and tested.

In order to establish the shear modulus G_{xz}, the assumptions of laminate theory are used. In composite laminate theory, a lamina with all its fibres orientated in a single direction is often analysed under states of in-plane stress. If the in-plane stresses are assumed to be in the xz plane with all the fibres orientated in the x direction, then the five elastic properties E_x, E_z, G_{xz}, v_{xz}, and v_{zx} can describe the elastic response of the material in any direction in the xz plane, and in particular, the elastic modulus in any direction in the lamina can then be established using Eq. 2, where θ is the angle between the direction of the fibres and the direction in which the elastic modulus is desired [13, 15].

$$\frac{1}{E} = \frac{\cos^2\theta}{E_x}\left(\cos^2\theta - v_{xz}\sin^2\theta\right) + \frac{\sin^2\theta}{E_z}\left(\sin^2\theta - v_{zx}\cos^2\theta\right) + \frac{\cos\theta^2\sin^2\theta}{G_{xz}} \tag{2}$$

In this work the analogy is drawn between the in-plane elastic response of the lamina (with fibres in the x direction) and the in-plane (xz plane) elastic response of the solid SLS fabricated samples (with layers in the x direction). Specifically, Eq. 2 is utilised to relate the elastic modulus in any direction in the xz place for the SLS samples to the five elastic properties and the angle of orientation [13]. In the experiments performed here, to

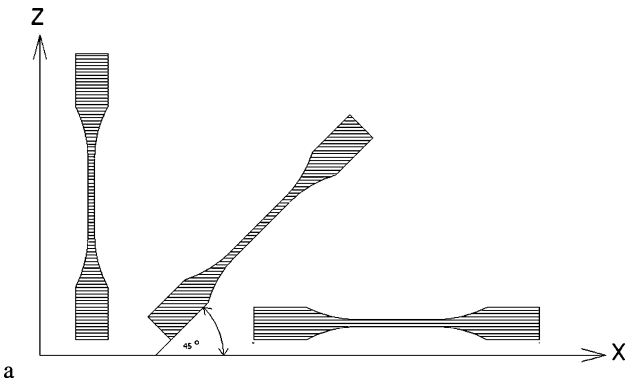

Fig. 8 To determine E_x and E_z solid specimen were fabricated with their longitudinal axis in the x and z directions. For the specimen fabricated at 45° to the xy plane, E_x and E_z were at 45° to the direction of loading. Using the results from these tests and Eq. 2 it was possible to determine the shear modulus G_{xz}

calculate the shear modulus, samples were fabricated at 45° to the xy plane (see Fig. 8). This meant that during tensile testing the principal elastic moduli E_x and E_z were at 45° to the direction of loading. As E_x, E_z, v_{xz}, and v_{zx} were already established from testing the solid samples in x and z direction, the results from these tensile tests (E) could be entered into Eq. 2 (with θ equal to 45°) to establish G_{xz}.

The PCL samples and the related FE model were assumed to be isotropic, as the only samples available were solid cylindrical samples which had been fabricated with their height in the z direction. The input data for elastic modulus in the FE model was taken from compression tests on these samples. To avoid discrepancies due to variance between scaffold builds, all solid samples used to collect input data for the FE model were fabricated in the same builds as the scaffolds that were tested.

3 Results and discussion

PCL and PA scaffolds were successfully fabricated using selective laser sintering. After the loose powder in the scaffold pores was removed, visual inspection showed all scaffolds to be open cellular structures with fully interconnected pores. Table 1 shows the porosity, pore size, strut thickness, and surface to volume ratio of the PCL and the PA scaffolds. For both scaffolds, the pore size was within the postulated ideal diameter range of 200–900 μm [11]. The PA scaffolds had a slightly higher porosity and more favourable surface to volume ratio; this was due to narrower struts been achieved in the PA scaffolds.

Mechanical testing of the solid PA samples showed that the assumption of transverse isotropy proved to be correct. The average elastic modulus for the scaffolds fabricated in x direction was just 1.3% lower than the average elastic modulus of the scaffolds fabricated in y direction, while the average elastic modulus of the scaffolds fabricated in the z direction were 16.4% lower than that of the scaffolds fabricated in the y direction. All values are listed in Table 2.

FE model predictions of effective moduli and the corresponding experimental measurements are given in Table 3. The FE model predicted the same effective moduli in tension and in compression for PA scaffolds in the x, y, and z directions. For the experiments, when compression and tension tests results were analysed, the biggest difference in the tensile effective modulus and the compressive effective modulus was for PA scaffolds tested in the y direction, and this was just 3%. For all scaffolds tested, the actual values for the effective moduli were found to be much lower than the FE predictions. The difference between actual and predicted values varied with the direction the effective modulus was measured. Table 3 shows that, for the compression samples, the FE model overpredicted the actual effective modulus by 81% for scaffolds loaded in the x direction, by 125% for scaffolds loaded in the y direction, and by 147% for scaffolds loaded in the z direction. Similar results can be seen for the PA tensile samples. For the PCL scaffold, the overprediction was 67%. In overall terms, even though both the scaffold geometry and material changed in going from the PA to the PCL, the results show that the difference between the measured and predicted values is on the same order of magnitude.

Figure 5 (considered above) shows a SEM image of a PA scaffold strut. Here it can be seen that in narrow struts, surface roughness can result in large variations in strut cross-section area. Figure 9 shows the Von Mises stress distribution for two FE scaffold models used to

Table 1 Geometrical properties of fabricated scaffolds

	Porosity	Average pore size	Average strut diameter	Surface to volume ratio
PA scaffold	56.4	600	350	3.58
PCL scaffold	55	659	431	3.42

Table 2 Results from mechanical testing of solid samples

	E_x (MPa)	E_y (MPa)	E_z (MPa)	G_{xz} (MPa)	v_{xz}	v_{zx}
PA samples	1770 ± 400	1794 ± 450	1500 ± 300	709 ± 90	0.3	0.3
PCL samples	–	–	47 ± 5	–	–	–

Table 3 FE predictions compared to experimental results for the effective modulus of the different scaffolds designs

Scaffolds	Experimental results (MPa)	FE prediction (MPa)	Degree of overprediction (%)
PCL	6 ± .9	10	67
Tensile PA (*x* direction)	190 ± 35	336	77
Tensile PA (*y* direction)	201 ± 40	439	118
Tensile PA (*z* direction)	180 ± 40	440	144
Compressive PA (*x* direction)	185 ± 15	336	81
Compressive PA (*y* direction)	195 ± 16	439	125
Compression PA (*z* direction)	178 ± 15	440	147

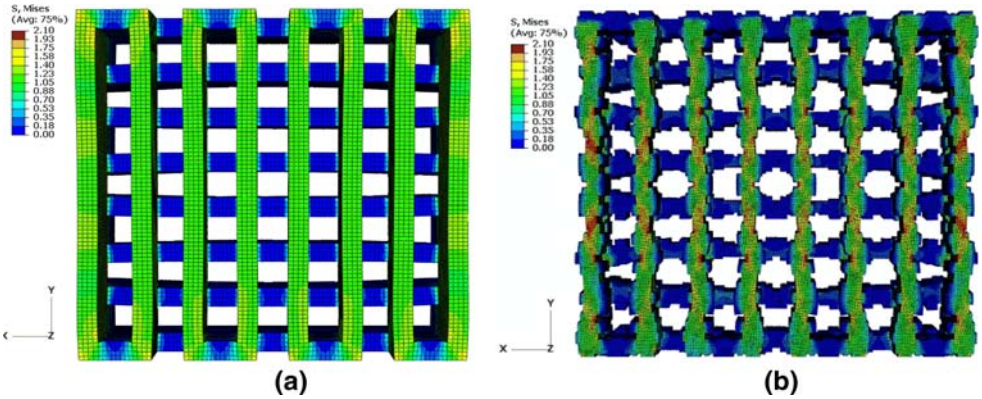

Fig. 9 Contour plot of von Mises stress distribution (MPa) for two scaffolds with exactly the same porosity that were compressed in the *y* direction. It was found that the effective modulus of the scaffold on the right was 68% higher that on the left

demonstrate the effects of roughness, loaded in compression. The model on the left (Fig. 9a) of a PA scaffold is of the type described above; the model on the right (Fig. 9b) is of the same material with the same porosity but with surface roughness induced by addition/removal of elements. Figure 10 shows a close up view of individual struts from the models of Fig. 9. As can be seen in Fig. 10, due to the surface roughness, a greater percentage of the rough scaffold structure experiences lower stress (dark blue elements) in comparison to the smooth scaffold structure, as the non-continuous paths in the struts do not contribute in taking up stress. These elements are deformed to a lower extent than the elements that experience high stress, and so contribute less to the overall stiffness of the scaffold. Correspondingly, the scaffold in Fig. 9a was predicted to have an effective modulus 66% higher than the scaffold in Fig. 9b, at 365 MPa compared to 220 MPa.

The SEM images also showed micropores to be present within the scaffold struts (Fig. 5). These can reduce the scaffold stiffness in two ways: (1) they are void areas and (2) they cause discontinuities in the struts meaning that some material near them will experience little stress.

Luxner et al. found that their FE analysis on the intended design of the PA scaffolds, fabricated by both SLS and Digital Light Processing (DLP) rapid prototyping techniques, overpredicted the effective modulus determined by

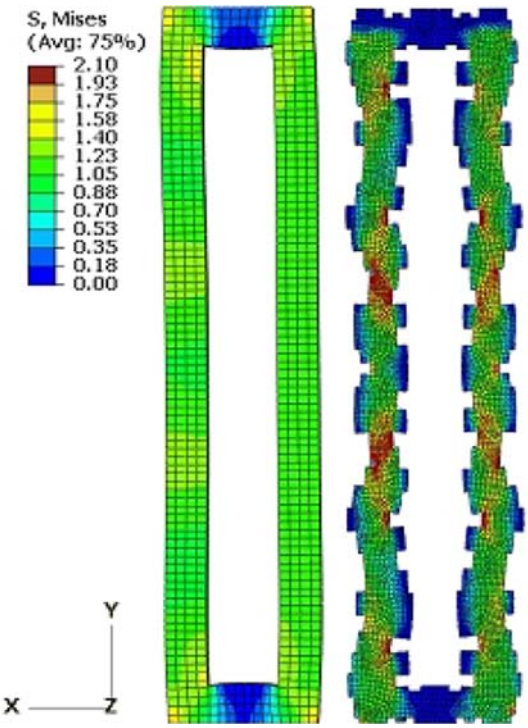

Fig 10 A comparison of stress distributions (MPa) of a smooth strut from Fig. 9a and a rough strut from Fig. 9b. The rough strut has a greater percentage of elements in violet. These elements contribute little to the scaffold's effective modulus

compression tests for scaffold structures with highly anisotropic mechanical properties by approximately 50 %, but that FE predictions were in good agreement to experimental results for scaffold structures with isotropic mechanical properties [6]. In this work, the degree of overprediction for the effective moduli in the FE analysis was different for the PCL scaffold and for each of the *x*, *y*, and *z* directions in the PA scaffold. These results suggest that microdefects, such as surface roughness and micropores, are significant, but have different levels of influence in different scaffold designs.

Selective Laser Sintering, like other rapid prototyping techniques, fabricates scaffolds based on 3D Computer Aided Design (CAD) models. For FEA to be useful in bone tissue engineering, it must be able to predict the performance of the scaffolds based on these models. For this reason, it is important to understand how surface roughness and micropores influence the scaffolds mechanical properties, and why this influence is different for different scaffold structures. As high resolution μCT scans would show the true extent to which surface roughness and micropores are present in fabricated scaffold structures, future work could involve image-based FE analysis being carried out on μCT scans of different scaffold designs and the results of this being compared with predictions from FE analysis based on the CAD model used to fabricate the scaffolds. Methodologies such as this should yield a clearer picture on how microdefects affect the mechanical properties of scaffolds, and which in turn could make FE predictions on scaffold mechanical performance more accurate.

4 Conclusions

Using PA and PCL, scaffolds with an open structure, pore sizes of 600 and 659 μm, and porosities of 56.4% and 55% were successfully fabricated using the SLS technique. To achieve these pore sizes, the scaffolds were fabricated with average strut diameters of 350 μm for the PA scaffolds and 431 μm for the PCL scaffolds. Comparisons of experimental results and FE predictions for mechanical properties showed that, at these diameters, features such as surface roughness and micropores can have a big influence on the scaffold's mechanical properties. Ignoring these features when developing FE models will lead to inaccurate predictions.

Acknowledgements The authors gratefully acknowledge the Programme for Research in Third Level Institutions (PRTLI), administered by the Higher Education Authority in Ireland. The authors also acknowledge the European Union and partners in the EU Framework Programme 6 Project "A Systems Approach to Tissue Engineering Processes & Products" (STEPS, Contract NMP3-CT-2005-500465, http://www.stepsproject.com/) for financial support of part of this study.

References

1. S.J. Hollister, C.Y. Lin, E. Saito, C.Y. Lin, R.D. Schek, J.M. Taboas, J.M. Williams, B. Partee, C.L. Flanagan, A. Diggs, E.N. Wilke, G.H. Van Lenthe, R. Muller, T. Wirtz, S. Das, S.E. Feinberg, P.H. Krebsbach, Orthod. Craniofac. Res. **8**, 162 (2005). doi:10.1111/j.1601-6343.2005.00329.x
2. D.W. Hutmacher, Biomaterials **21**, 2529 (2000). doi:10.1016/S0142-9612(00)00121-6
3. S.J. Hollister, R.D. Maddox, J.M. Taboas, Biomaterials **23**, 4095 (2002). doi:10.1016/S0142-9612(02)00148-5
4. D.L. Butler, S.A. Goldstein, F. Guilak, Trans ASME **122**, 570 (2000)
5. J.M. Williams, A. Adewunmi, R.M. Schek, C.L. Flanagan, P.H. Krebsbach, S.E. Feinberg, S.J. Hollister, S. Das, Biomaterials **26**, 4817 (2005). doi:10.1016/j.biomaterials.2004.11.057
6. M.H. Luxner, J. Stampfl, H.E. Pettermann, J. Mater. Sci. **40**, 5859 (2005). doi:10.1007/s10853-005-5020-y
7. C.M. Cheah, C.K. Chua, K.R. Leong, S.W. Chua, Int. J. Adv. Manuf. Technol. **21**, 302 (2003). doi:10.1007/s001700300035
8. D.W. Hutmacher, T. Schantz, I. Zein, K.W. Ng, S.H. Teoh, K.C. Tan, J. Biomed. Mater. Res. **55**, 203 (2001). doi:10.1002/1097-4636(200105)55:2<203::AID-JBM1007>3.0.CO;2-7
9. M.A. Wettergreen, B.S. Bucklen, B. Starly, E. Yuksel, W. Sun, M.A.K. Liebschner, Computer-Aided Des. **37**, 1141 (2005). doi:10.1016/j.cad.2005.02.005
10. K. Whang, K.E. Healy, D.R. Elenz, E.K. Nam, D.C. Tsai, C.H. Thomas, G.W. Nuber, F.H. Glorieux, R. Travers, S.M. Sprague, Tissue Eng. **5**, 35 (1999). doi:10.1089/ten.1999.5.35
11. A.J. Salgado, O.P. Coutinho, R.L. Reis, Macromol. Biosci. **4**, 743 (2004). doi:10.1002/mabi.200400026
12. S. Lohfeld, M.A. Tyndyk, S. Cahill, N. Flaherty, P.E. McHugh, V. Barron, Rapid Prototyp J. (submitted)
13. Caulfield B, Investigation of the Material Properties of Parts Produced using the SLS Rapid Prototyping Process, Masters thesis, National University of Ireland Galway, Galway, 2004, p. 42
14. B. Caulfield, P.E. McHugh, S. Lohfeld, J. Mater. Process. Technol. **182**, 477 (2007). doi:10.1016/j.jmatprotec.2006.09.007
15. R.J. Crawford, *Plastics Engineering* (Elsevier Butterworth-Heinemann, Oxford, 1998), p. 182